Detailed traveltime tomography and seismicity around the 2019 M7.1 Ridgecrest, CA, earthquake using dense rapid-response seismic data

Malcolm C. A. White[1] Hongjian Fang[2] Rufus D. Catchings[3] Mark R. Goldman[3] Jamison Steidl[4] Yehuda Ben-Zion[1,5]

[1]University of Southern California [2]Massachusetts Institute of Technology [3]United States Geological Survey [4]University of California Santa Barbara [5]Southern California Earthquake Center

Overview

We process raw waveform data using automated procedures to derive an independent earthquake catalog and high-resolution models of seismic velocity structure (v_P, v_S, and v_P/v_S) in the region surrounding the 2019 M_w7.1 Ridgecrest, CA earthquake using recordings of the aftershock sequence from a rapid-response dense deployment of geophones.

1. Data

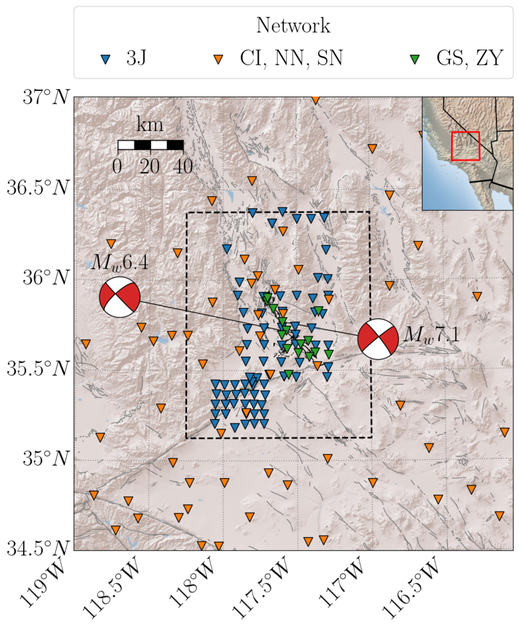

Figure 1: Map of 152 seismic sensors used in this study: (a) 78 dense-deployment geophones from the 3J network (blue triangles); (b) 55 permanent broadband stations from the CI, NN, and SN networks (orange triangles); and (c) 15 temporary broadband seismometeres from the GS and ZY networks (green triangles). The black dashed rectangle outlines the focus region of this study.

2. Methods

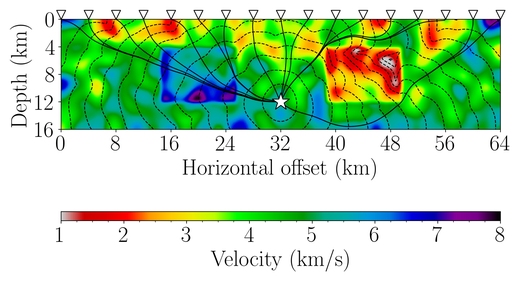

Figure 2: Synthetic wavefronts emanating from a point source (white star) at half-second intervals (black dashed curves) and raypaths (solid black curves) through heterogeneous velocity structure. We use PyKonal (White et al., 2020) to solve the forward problem when inverting for earthquake locations and velocity structure.

3. Results

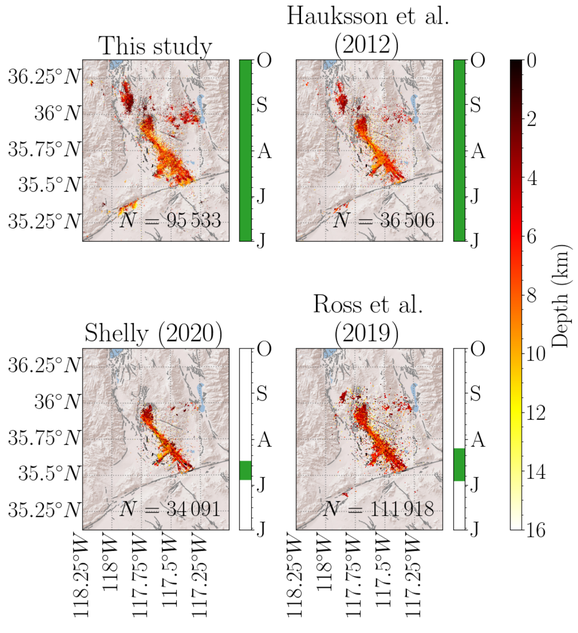

Figure 3: Event maps for four different catalogs. The green filled areas in the vertical bars to the right of each map indicate temporal coverage of the corresponding catalog; letters represent the beginning of successive months (June, July, August, September, and October). The number of events, N, is indicated at the bottom right of each map.

3.1 P-wave velocity structure

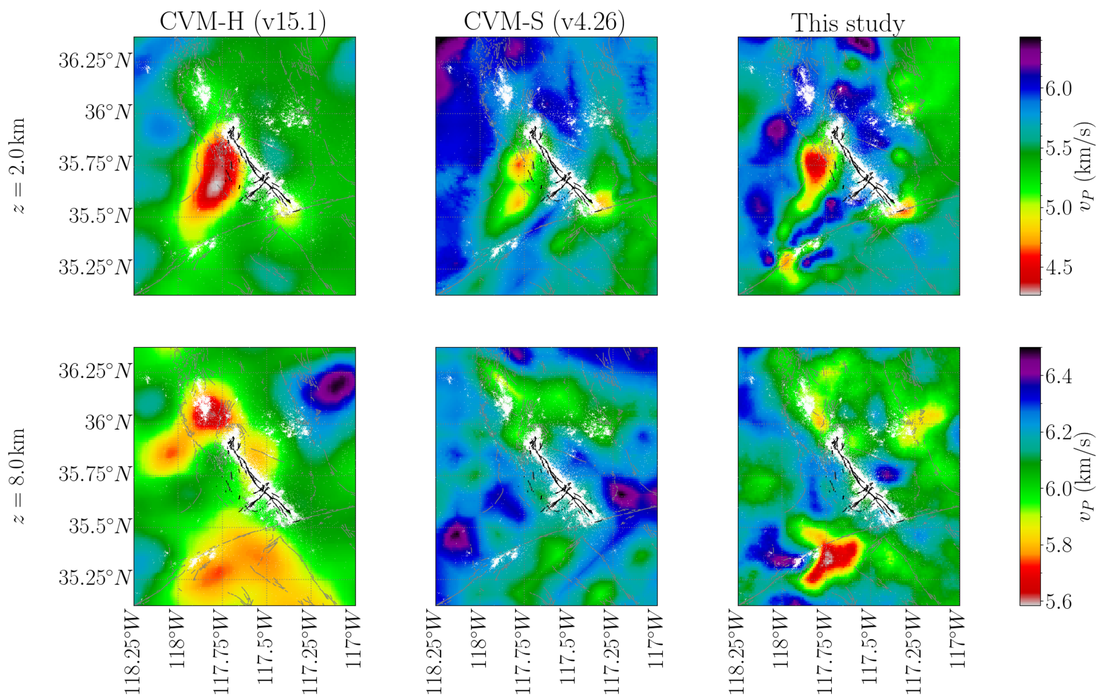

Figure 4: P-wave velocity structure at 2 km (top row) and 8 km (bottom row) below sea level as modeled by SCEC CVM-H15.1 (left column), CVM-S4.16 (middle column), and this study (right column). Solid gray and black lines show surface traces of Quarternary faults and faults activated during the 2019 Ridgecrest earthquake sequence, respectively. White dots indicate earthquake epicenters.

3.2 S-wave velocity structure

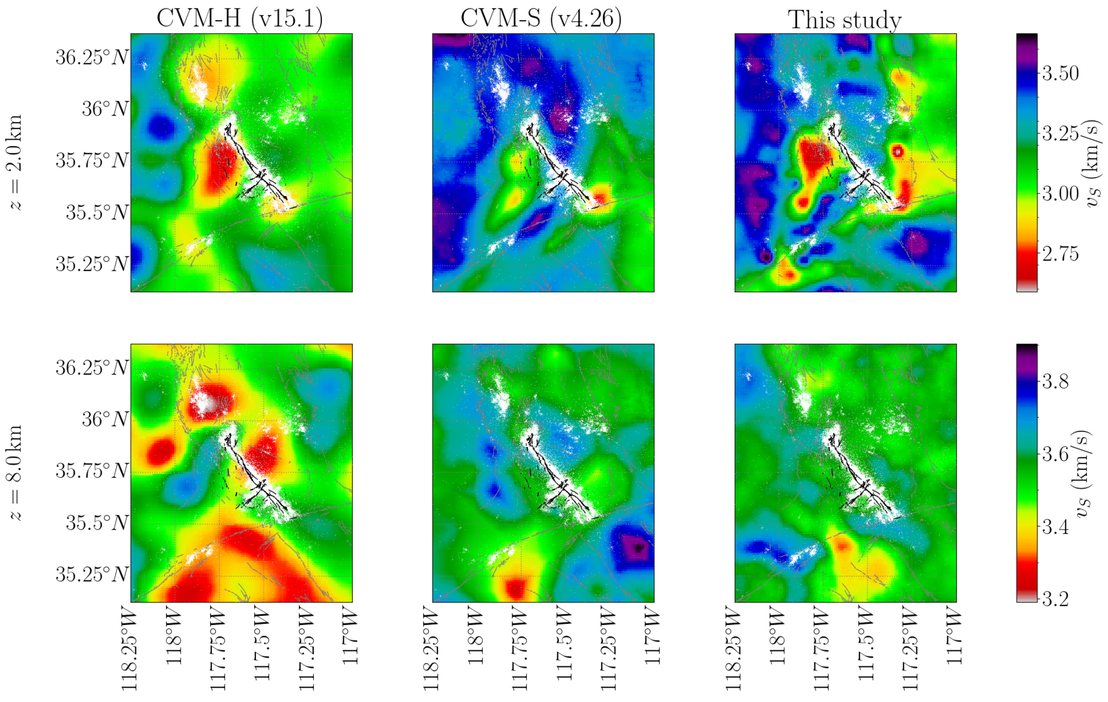

Figure 5: S-wave velocity structure as in Figure 4.

Main conclusions

1. We process raw waveform data using automated procedures to derive a catalog of over 95 000 earthquakes that is independent of any *a priori* observations.
2. We obtain fully 3D event locations using the Differential Evolution algorithm (Storn & Price, 1997) and robust PyKonal raytracer (White et al., 2020).
3. We invert our catalog for v_P, v_S, and v_P/v_S structure using a traveltime tomography method based on Poisson-Voronoi projections (Fang et al., 2020).
4. We observe (a) strong correlations between surface geology and shallow velocity structure; (b) low v_P at the base of the seismogenic zone; and (c) low v_S beneath the Coso volcanic field.

3.3 Surface geology

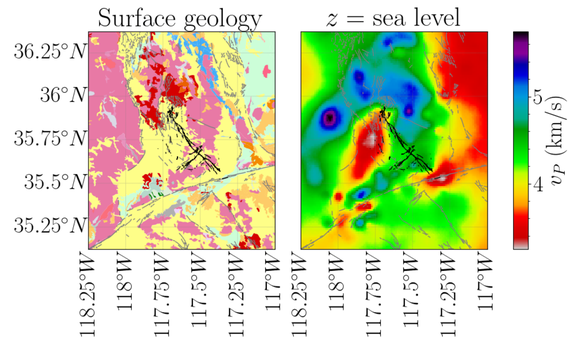

Figure 6: Surface geology (left panel) and P-wave velocity structure at sea level (850 m below average station elevation). Solid gray and black lines indicate fault traces as in Figure 4.

3.4 Vertical transects

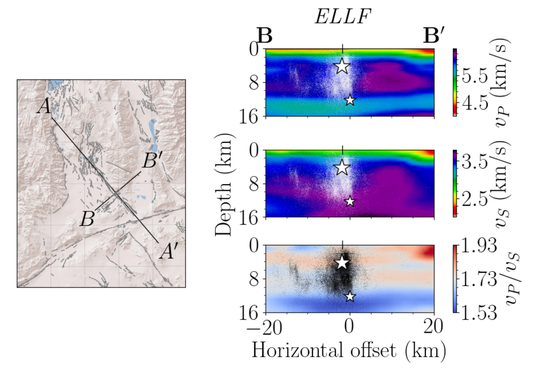

Figure 7: Map indicating surface traces (solid black lines) of vertical transects $A-A'$ and $B-B'$ (left panel). v_P (top right panel), v_S (middle right panel), and v_P/v_S (bottom right panel) structure along vertical transect $B-B'$. Black and white dots represent earthquakes within ±10 km of the $B-B'$ plane projected onto the plane. White stars indicate the projected hypocenters of the M_w7.1 (larger shallower star) and M_w6.4 earthquakes.

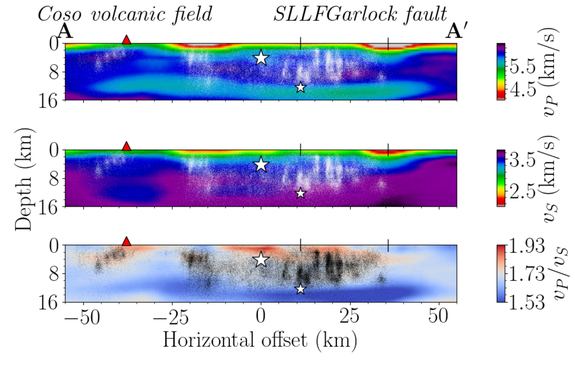

Figure 8: Velocity structure along transect $A-A'$ as in the right column of Figure 7.

References

California Institute of Technology, & United States Geological Survey Pasadena. (1926). *Southern California Seismic Network*. doi: 10.7914/SN/CI

Fang, H., van der Hilst, R. D., de Hoop, M. V., Kothari, K., Gupta, S., & Dokmanić, I. (2020). Parsimonious Seismic Tomography with Poisson Voronoi Projections: Methodology and Validation. *Seismological Research Letters*, *91*(1), 343–355. doi: 10.1785/0220190141

Hauksson, E., Yang, W., & Shearer, P. M. (2012). Waveform Relocated Earthquake Catalog for Southern California (1981 to June 2011). *Bulletin of the Seismological Society of America*, *102*(5), 2239–2244. doi: 10.1785/0120120010

Lee, E., Chen, P., Jordan, T. H., Maechling, P. B., Denolle, M. A. M., & Beroza, G. C. (2014). Full-3-D tomography for crustal structure in Southern California based on the scattering-integral and the adjoint-wavefield methods. *Journal of Geophysical Research: Solid Earth*, *119*(8), 6421–6451. doi: 10.1002/2014JB011346

Ponti, D. J., Blair, J. L., Rosa, C. M., Thomas, K., Pickering, A. J., Akciz, S., … Zinke, R. (2020). Documentation of Surface Fault Rupture and Ground-Deformation Features Produced by the 4 and 5 July 2019 Mw 6.4 and Mw 7.1 Ridgecrest Earthquake Sequence. *Seismological Research Letters*(July 2019). doi: 10.1785/0220190322

Ross, Z. E., Idini, B., Jia, Z., Stephenson, O. L., Zhong, M., Wang, X., … Jung, J. (2019). Hierarchical interlocked orthogonal faulting in the 2019 Ridgecrest earthquake sequence. *Science*, *366*(6463), 346–351. doi: 10.1126/science.aaz0109

Shaw, J. H., Plesch, A., Tape, C., Suess, M. P., Jordan, T. H., Ely, G., … Munster, J. (2015). Unified Structural Representation of the southern California crust and upper mantle. *Earth and Planetary Science Letters*, *415*, 1–15. doi: 10.1016/j.epsl.2015.01.016

Shelly, D. R. (2020). A High-Resolution Seismic Catalog for the Initial 2019 Ridgecrest Earthquake Sequence: Foreshocks, Aftershocks, and Faulting Complexity. *Seismological Research Letters*, *91*(4), 1971–1978. doi: 10.1785/0220190309

Steidl, J., Catchings, R., & Allam, A. (2019). *RAMP deployment of 3C nodal for July Searles Valley 2019 Earthquake*. International Federation of Digital Seismograph Networks. doi: 10.7914/SN/3J_2019

Storn, R., & Price, K. (1997). Differential Evolution – A Simple and Efficient Heuristic for Global Optimization over Continuous Spaces. *Journal of Global Optimization*, *11*(4), 341–359. doi: 10.1023/A:1008202821328

University of Nevada, Reno. (1971). *Nevada Seismic Network*. International Federation of Digital Seismograph Networks. doi: 10.7914/SN/NN

University of Nevada, Reno. (1980). *Southern Great Basin Network*. International Federation of Digital Seismograph Networks. doi: 10.7914/SN/SN

White, M. C. A., Fang, H., Nakata, N., & Ben-Zion, Y. (2020). PyKonal: A Python Package for Solving the Eikonal Equation in Spherical and Cartesian Coordinates Using the Fast Marching Method. *Seismological Research Letters*, *91*(4), 2378–2389. doi: 10.1785/0220190318